文章编号:1004-7220(2009)05-0352-10

Transient elastohydrodynamic lubrication analysis of a novel metal-on-metal hip prosthesis with an aspherical acetabular bearing surface

Qingen Meng[1], Leiming Gao[1], Feng Liu[1], Peiran Yang[2], John Fisher[1], Zhongmin Jin[1] *1.Institute of Medical and Biological Engineering,School of Mechanical Engineering, University of Leeds, Leeds, LS2 9JT, UK;2. School of Mechanical Engineering, Qingdao Technological University, Qingdao, 266033, China*

Abstract: Objective To investigate the EHL performance of a novel prosthesis employing Alpharabola cup under realistic walking conditions. **Method** A transient elastohydrodynamic lubrication model was created for this novel hip prosthesis. A normal walking gait was represented by the ISO specified dynamic operation conditions. Complete numerical solutions were obtained by solving the Reynolds equation in spherical coordinates, the film thickness equation and the load balance equations using Multi-grid technologies. **Result** Detailed variations in film profile and pressure distribution during one convergent walking cycle were analyzed. The effect of parameter α on quasi-static and transient solutions of the central and minimum film thicknesses and maximum pressures was investigated. The transient and quasi-static solutions for the same parameter α were compared. The lubrication performance of Alpharabola hip prostheses and that of a spherical hip prosthesis were compared under both transient and quasi-static conditions. **Conclusions** It was found that both the squeeze film action and the non-spherical acetabular surface can significantly improve lubrication performance under realistic walking conditions, in increasing the predicted lubricant film thickness and decreasing the maximum hydrodynamic pressure. The metal-on-metal Alpharabola hip prosthesis was shown to benefit from fluid film lubrication significantly more than spherical hip prostheses.

Key words: Transient elastohydrodynamic lubrication; Metal-on-metal hip prostheses; Non-spherical bearing surfaces; Alpharabola acetabular surface

一种使用非球面髋臼的金属-金属髋关节假体的时变弹流润滑分析

孟庆恩[1]， 高雷鸣[1]， 刘 峰[1]， 杨沛然[2]， John Fisher[1]， 靳忠民[1]
（1. 利兹大学 机械工程学院 医药与生物工程研究所；2. 青岛理工大学 机械工程学院）

摘要：目的 研究使用 Alpharabola 型髋臼的新型髋关节假体在实际步态条件下的弹性流体动力润滑（弹流）性能。**方法** 建立了该新型髋关节假体的非稳态 EHL 模型。用 ISO 规定的动载运动条件表示一个常态的步态。利用多重网格技术，求解球坐标系下的雷诺方程、膜厚方程和载荷方程以获得完全数值解。**结果** 分析了一个收敛的步态中润滑油膜形状和压力分布的详细变化。研究了参数 α 对中心膜厚、最小膜厚和中心压力的准稳态和非稳态解的影响。比较了相同参数 α 的准稳态解和非稳态解。在非稳态和准稳态条件下，比较了 Alpharabola 型髋关节假体和球形髋关节假体的润滑性能。**结论** 结果发现，在实际步态条件下，挤压膜效应和非球形髋臼表面两者都能显著提高润滑性能，即能够使油膜增厚，最大压力减小。和球形人工髋关节相比，Alpharabola 型金属-金属人工髋关节更能得益于全膜流体润滑。

收稿日期:2009-10-09
作者简介:孟庆恩(1978-)，博士，研究方向:生物摩擦学。
通讯作者:孟庆恩，Tel: 44 113 242 4611；E-mail: mnqm@ leeds.ac.uk.

关键词：时变弹流润滑；金属-金属髋关节假体；非球形轴承表面；Alpharabola 髋臼表面
中图分类号：R318.01　　文献标志码：A

1 Introduction

Hip joint connects the lower limbs to the trunk by a ball-in-socket articulation, which can be viewed as a remarkable bearing in the human body in engineering terms. Such a bearing is expected to function in the body for a lifetime whilst transmitting large dynamic loads and providing a wide range of movements. Therefore, when osteoarthritis, rheumatoid arthritis or trauma causes it to fail to function properly, the individual's life style is severely impaired. Hip joint arthroplasty has been regarded as the most successful surgical treatment to hip joint diseases in the past century. More recently, a significant development of the metal-on-metal (MOM) bearing combination has been witnessed due to its exceedingly low wear rate[1]. Since the metallic wear particles are nanometers in size and high in numbers, they are very easy to be absorbed by the joint tissues and disseminated to other organs[2,3]. Therefore, in order to avoid the potential risk of adverse biological reactions, it is still necessary to minimize wear in MOM hip prostheses.

Lubrication study plays an important role in minimizing wear of MOM hip prosthesis since an effective lubricant film in hip prostheses can sustain the external load between the bearing surfaces while avoid direct asperity contacts. Thereby the wear of the two bearing surfaces may be mainly governed by the viscous characteristics of the synovial fluid in the joints. Diameter and diametral clearance of MOM hip prosthesis have been found to be important parameters for improving lubrication[4-6]. Moreover, flexible structural supports, such as the polyethylene backing underneath the metallic bearing in the Metasul bearing system and the taper connection in the Ultima prosthesis, can also improve the film thickness by increasing the elastic deformation[7,8].

Although reducing clearance is an important design consideration in wear reduction in MOM hip prostheses, it is limited by a number of practical factors, such as the requirement of tighter manufacturing accuracy, the potential clamping and equatorial contact under loading and when implanted through press-fit[9], etc. An excessively small clearance may also result in a drastic increase in wear and frictional torque[10,11]. On the other hand, MOM hip prosthesis bearings exhibit biphasic wear, an initial running-in or bedding-in phase with a higher wear rate, followed by a steady-state phase at a lower wear rate[12,13]. It is widely believed that during the running-in wear phase, the two bearing surfaces of the hip prosthesis are slowly modified by wear, forming more conforming bearing surfaces in the worn area[14,15]. The running-in wear in MOM hip prostheses implies that spherical bearings are not optimal from a lubrication point of view. Within the worn patch, the clearance between the two bearing surfaces is significantly reduced, compared with the initial value. This produces a geometry that is more favorable to fluid film lubrication [13]. When fluid film lubrication prevails, the wear during the steady-state phase occurs at a slower rate. Therefore, it is reasonable to assume that the optimized MOM bearing surfaces should resemble those of the worn bearing surfaces after the running-in wear.

Therefore, it is only necessary to reduce the clearance of the MOM bearings within the main loaded area, while it is advantageous to increase the clearance in the equatorial region. Such a variable clearance can be achieved through using an aspherical bearing surface for either acetabular cup or femoral head. Alpharabola acetabular cup surface[16,17] is one of such examples. The contact mechanics and elastohydrodynamic lubrication (EHL) of a novel hip prosthesis with an Alpharabola acetabular cup under steady-state operating conditions have been studied and the lubrication advantages of the Alpharabola cup surface over a spherical surface have been found[17]. The purpose of this study was to investigate the transient EHL of this novel hip prosthesis under dynamic load and motion specified by ISO standard.

2 Lubrication Model and Methods

2.1 Model

Since the effect of the inclination angle of the cup on lubrication performance is negligible throughout the normal walking cycle[18], the cup was positioned horizontally instead of inclined anatomically as shown in Fig.1. An Alpharabola surface was applied as the surface of the acetabular cup, which was defined as Eq. (1)[17]:

$$\frac{x^2}{R_2^2/\alpha}+\frac{(y-R_2+R_2/\alpha)^2}{R_2^2/\alpha^2}+\frac{z^2}{R_2^2/\alpha}=1,0<\alpha<1 \quad (1)$$

where x, y and z are Cartesian coordinates defined in Figs. 1 and 2. R_2 is the desired minimum radius of curvature of the cup; α is a parameter to control the variation rate of the radius of the curvature. Only the portion of the surface within $0\leqslant y\leqslant R_2$ was employed. The radius of the femoral head, R_1, was equal to R_2 to produce a local zero radial clearance at the pole. A relatively larger clearance at the equatorial region, $(\sqrt{2-\alpha}-1)R_2$, was formed by the variation of the radius of the cup.

Both femoral head and acetabular cup of this prosthesis were assumed to be made of CoCr alloy. The cup thickness of 9.5 mm for a typical 28 mm total hip replacement (THR) was adopted. The effect of bone and fixation was represented by an equivalent support layer of thickness of 2 mm[19]. The lubricant in artificial hip joints is periprosthetic synovial fluid, which was assumed as Newtonian, isoviscous and incompressible[20,21]. Therefore a realistic viscosity of 0.002 Pa s was adopted to

simulate the *in-vivo* conditions. The geometric and mechanical parameters of the transient EHL model of Alpharabola hip prostheses are summarized in Tab.1.

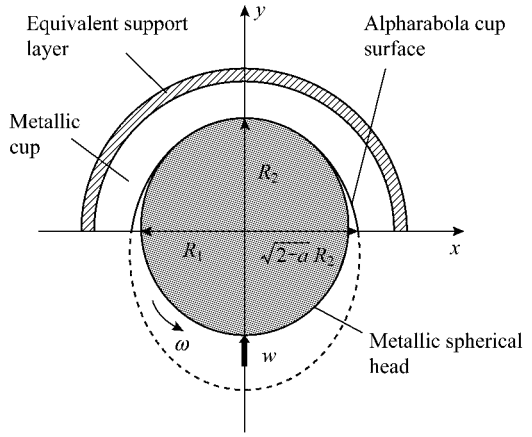

Fig.1 A simple ball-in-socket configuration for the MOM hip prosthesis employing Alpharabola as the bearing surface of the cup

图1 简化的 Alpharabola 型金属-金属人工髋关节示意图

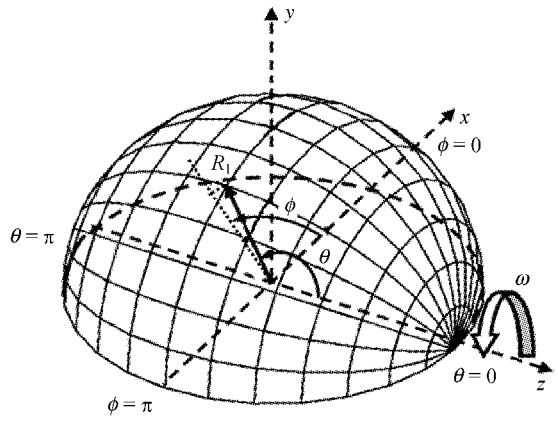

Fig.2 Definition of spherical coordinates and mesh grid on a given level[18]

图2 球坐标的定义和给定层上的网格划分[18]

Tab.1 Typical geometric and physical parameters adopted in this study for the transient EHL model of Alpharabola hip prostheses

表1 Alpharabola 人工髋关节的时变弹流模型的典型的几何和力学参数

Thickness of equivalent support	2 mm
α	0.9957, 0.99, 0.97
Minimum radius of cup inside surface, R_2	14 mm
Radius of head, R_1	14 mm
Cup wall thickness	9.5 mm
Elastic modulus of the metal	210 GPa
Elastic modulus of equivalent support	2.27 GPa
Poisson's ratio of metal	0.3
Poisson's ratio of equivalent support	0.23
Viscosity of synovial fluid	0.002 Pa s

In reality, both the load and motion experienced in human hip joints are three-dimensional and time-dependent[22]. In this study, the dynamic operation conditions of normal walking specified by the ISO testing standard[23] were adopted. Since the major velocity component is in flexion/extension direction, only the rotation velocity around the *z* axis, ω, was considered[7], as shown in Fig.3. In addition, the load applied was in the vertical direction.

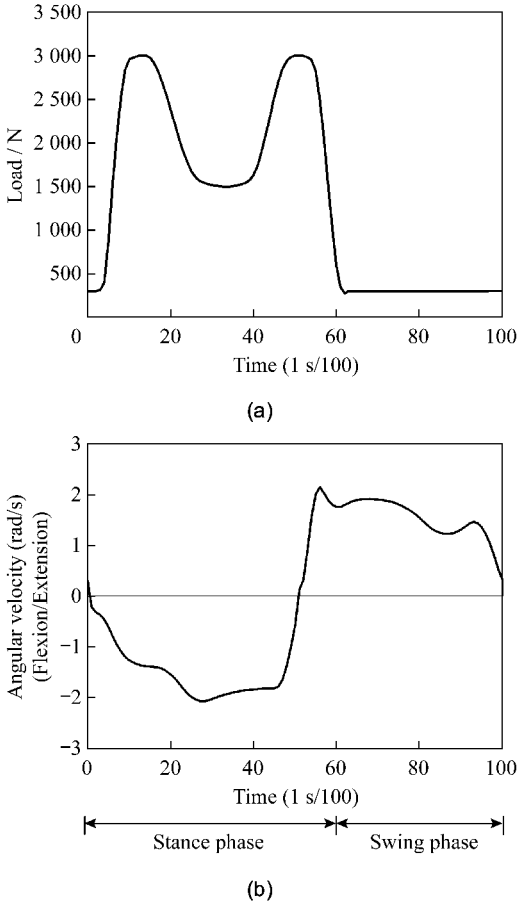

Fig.3 Variation of the dynamic load (a) and velocity (b) within a walking gait specified by ISO standard

图3 ISO 规定的一个步态中载荷 (a) 和速度 (b) 变化

2.2 Governing equations

The governing equation for the hydrodynamic action between the two bearing surfaces is the Reynolds equation, which took the following form in the spherical coordinates for the present study:

$$\sin\theta\frac{\partial}{\partial\theta}\left(h^3\sin\theta\frac{\partial p}{\partial\theta}\right)+\frac{\partial}{\partial\phi}\left(h^3\frac{\partial p}{\partial\phi}\right)=6\eta R_1^2\sin^2\theta\left(\omega\frac{\partial h}{\partial\phi}+2\frac{\partial h}{\partial t}\right) \quad (2)$$

where p is the hydrodynamic pressure; h is the film thickness; η is the viscosity of the periprosthetic synovial fluid; t is time; ω is the angular velocity of the femoral head; ϕ and θ are spherical coordinates, as defined in Fig. 2.

The boundary conditions at any instant were the same as those of a steady-state EHL problem:

$$p(0,\theta) = p(\pi,\theta) = p(\phi,0) = p(\phi,\pi) = 0$$

$$\partial p/\partial\phi = \partial p/\partial\theta = 0,\quad 0 < \phi < \pi,\quad 0 < \theta < \pi$$

The film thickness consisted of the undeformed gap and the elastic deformation of bearing surfaces due to the hydrodynamic pressure:

$$h = R_c(\theta,\phi) - R_1 - e_x\sin\theta\cos\phi - e_y\sin\theta\sin\phi + \delta \quad (3)$$

where e_x and e_y are eccentricities of the femoral head; δ is the elastic deformation of bearing surfaces; $R_c(\theta,\phi)$ is the varying radius of the aspherical cup, which was calculated by substituting the following equations

$$x = R_c\sin\theta\cos\phi,\ y = R_c\sin\theta\sin\phi,\ \text{and } z = R_c\cos\theta$$

into Eq.(1), then solving the resultant quadratic equation with R_c as unknowns.

In addition, the external load components, f_x, f_y and f_z, were balanced by the integration of the hydrodynamic pressure:

$$f_x = R_1^2\int_0^{\pi}\int_0^{\pi} p\sin^2\theta\cos\phi\,d\theta\,d\phi = 0 \quad (4)$$

$$f_y = R_1^2\int_0^{\pi}\int_0^{\pi} p\sin^2\theta\sin\phi\,d\theta\,d\phi = w_y \quad (5)$$

$$f_z = R_1^2\int_0^{\pi}\int_0^{\pi} p\sin\theta\cos\phi\,d\theta\,d\phi = 0 \quad (6)$$

Since only the vertical load and the flexion/extension motion were considered, Eq. (6) was satisfied automatically.

2.3 Numerical method

In order to facilitate the numerical analysis and improve the stability of the numerical process, the governing equations used in the present study were non-dimensionalised using the following definitions:

$$H = \frac{h}{c},\ \Delta = \frac{\delta}{c},\ P = \frac{p}{E},\ T = t\omega_0,\ \lambda = \frac{6\eta R_1^2\omega_0}{c^2E},$$

$$\bar{\omega} = \omega/\omega_0,\ W = \frac{w}{ER_1^2},\ \overline{f_x} = \frac{f_x}{ER_1^2},\ \overline{f_y} = \frac{f_y}{ER_1^2} \quad (7)$$

where E is the elastic modulus of the material of cup and head. Theoretically, ω_0 and c can be any constant except zero. In this study, ω_0 was chosen as 2 rad/s and c was chosen as the radial clearance at the equatorial region, $(\sqrt{2-\alpha}-1)R_2$.

The governing equations after non-dimensionalised were written as respectively,

$$\sin\theta\frac{\partial}{\partial\theta}\left(H^3\sin\theta\frac{\partial P}{\partial\theta}\right) + \frac{\partial}{\partial\phi}\left(H^3\frac{\partial P}{\partial\phi}\right) = \lambda\sin^2\theta\left(\bar{\omega}\frac{\partial H}{\partial\phi} + 2\frac{\partial H}{\partial T}\right) \quad (8)$$

$$H = \frac{R_c - R_1}{c} - \varepsilon_x\sin\theta\cos\phi - \varepsilon_y\sin\theta\sin\phi + \Delta \quad (9)$$

$$\overline{f_x} = \int_0^{\pi}\int_0^{\pi} P\sin^2\theta\cos\phi\,d\theta\,d\phi = 0 \quad (10)$$

$$\overline{f_y} = \int_0^{\pi}\int_0^{\pi} P\sin^2\theta\cos\phi\,d\theta\,d\phi = W \quad (11)$$

A walking cycle was divided into 100 instants. At each instant the numerical technique was similar to that of a steady-state solution. In brief, the Reynolds equation was solved with a multi-grid method; the elastic deformation was calculated using a multi-level multi-integration technique[24]; the load balance was satisfied through adjusting the eccentricity ratios of x and y. The detailed description of the numerical method is as following.

The calculation domain was divided into different grids on different levels. The Reynolds equation (8) was discretized with a finite difference scheme into the same form on each level of grids. At each non-boundary node, when the superscript k was used to denote the grid level, and subscripts i, j were used as nodal numbers in the ϕ and θ directions respectively, using the central finite difference approximation to the left-hand side of Eq.(8) and the backward finite difference to the right-hand side, the Reynolds equation (8) was written as

$$(L_0\boldsymbol{P}^k)_{ij} = F_{ij}^k \quad (12)$$

In detail,

$$\frac{\sin\theta_j^k}{(\Delta\theta^k)^2}[(\varepsilon_{i,j-1/2}^k\sin\theta_{j-1/2}^k)P_{i,j-1}^k - (\varepsilon_{i,j-1/2}^k\sin\theta_{j-1/2}^k + \varepsilon_{i,j+1/2}^k\sin\theta_{j+1/2}^k)P_{ij}^k + (\varepsilon_{i,j+1/2}^k\sin\theta_{j+1/2}^k)P_{i,j+1}^k] + \frac{1}{(\Delta\phi^k)^2}[(\varepsilon_{i-1/2,j}^k P_{i-1,j}^k - (\varepsilon_{i-1/2,j}^k + \varepsilon_{i+1/2,j}^k)P_{ij}^k + \varepsilon_{i+1/2,j}^k + P_{i+1,j}^k] - \bar{\omega}\sin^2\theta_j^k\frac{H_{ij}^k - H_{i-1,j}^k}{\Delta\phi^k} - 2\sin^2\theta_j^k\frac{H_{ij}^k}{\Delta T} = F_{ij}^k \quad (13)$$

where $\varepsilon = H^3/\lambda$, and

$$\varepsilon_{i\pm1/2,j}^k = (\varepsilon_{i\pm1,j}^k + \varepsilon_{ij}^k)/2,\quad \varepsilon_{ij\pm1/2}^k = (\varepsilon_{ij\pm1}^k + \varepsilon_{ij}^k)/2,$$
$$\theta_{j\pm1/2}^k = (\theta_{j\pm1}^k + \theta_j^k)/2$$

Furthermore, $\Delta\theta^k$ and $\Delta\phi^k$ are the mesh lengths in the θ,ϕ directions on grid level k respectively, and ΔT is the time interval.

The discretized film thickness equation was

$$H_{ij}^k = \frac{R_c - R_1}{c} - \varepsilon_x\sin\theta_j^k\cos\phi_i^k - \varepsilon_y\sin\theta_j^k\sin\phi_i^k + \sum_{k1=0}^{n_\phi^k}\sum_{l=0}^{n_\theta^k} K_{i,j,k1,l}P_{k1,l}^k \quad (14)$$

where n_θ^k and n_ϕ^k are the numbers of nodes on level k in θ and ϕ directions respectively; $K_{i,j,k1,l}$ is the elastic deformation coefficient, representing the summation of the elastic deformation of both cup and head at node (i, j) resulting from the unit pressure at node $(k1, l)$. The deformation coefficients of the Alpharabola cup were approximated by those of a spherical cup with a radius given by the minimum radius of the Alpharabola cup[17,25].

In order to simplify the writing of the discretized load equations, the Simpson's quadrature on level r was defined as

$$\int_0^{\pi}\int_0^{\pi} U^r\,d\theta\,d\phi = \frac{1}{9}\Delta\phi^r\Delta\theta^r\sum_{i=0}^{n_\phi^r/2-1}\sum_{j=0}^{n_\theta^r/2-1}[16U_{2i+1,2j+1}^r + 4(U_{2i+1,2j}^r + U_{2i+1,2j+2}^r + U_{2i,2j+1}^r + U_{2i+2,2j+1}^r) + U_{2i,2j}^r + U_{2i+2,2j}^r + U_{2i,2j+2}^r + U_{2i+2,2j+2}^r] \quad (15)$$

then the load equations were discretized as follows on level k

$$\overline{f_x^k} = \int_0^{\pi}\int_0^{\pi} Q^k\,d\theta\,d\phi = g_x^k \quad (16)$$

$$\overline{f_y^k} = \int_0^{\pi}\int_0^{\pi} S^k\,d\theta\,d\phi = g_y^k \quad (17)$$

where

$$Q = P\sin^2\theta\cos\phi,\ S = P\sin^2\theta\sin\phi$$

Only on the finest level of grid (i.e. when $k=m$), the right-hand side terms for Eqs. (12), (16) and (17). were derived from the discretized Reynolds and load equations as

$$F_{i,j}^k = -2\sin^2\theta_j^k \frac{(H_{i,j}^k)^{T-\Delta T}}{\Delta T} \tag{18}$$

$$g_x^k = 0,\ g_y^k = W \tag{19}$$

where the superscript $T-\Delta T$ denotes the previous instant. On all the other levels, the right-hand side terms were determined from the relaxation results on the upper level through an operator of restriction.

$$\boldsymbol{F}^{k-1} = L^{k-1}(I_k^{k-1}\tilde{\boldsymbol{P}}^k) + I_k^{k-1}(\boldsymbol{F}^k - L^k\tilde{\boldsymbol{P}}^k) \tag{20}$$

where $\tilde{\boldsymbol{P}}^k$ is the solved vector of nodal pressures on the current level and I_k^{k-1} is the operator of restriction from the current level to the lower level.

Pressure relaxation was carried out on each level using the following iterative scheme

$$\tilde{P}_{i,j}^k = \bar{P}_{i,j}^k + \omega_P\delta P_{i,j}^k \tag{21}$$

where ω_P is the under-relaxation factor; $\delta P_{i,j}^k$ was calculated from a local Newton-Raphson scheme:

$$\delta P_{i,j}^k = \frac{r_{i,j}^k}{(\partial L_{i,j}/\partial P_{i,j})^k} \tag{22}$$

At a typical inner node, the formulae for $r_{i,j}^k$ and $(\partial L_{i,j}/\partial P_{i,j})^k$ were

$$r_{i,j}^k = F_{i,j}^k - \frac{\sin\theta_j^k}{(\Delta\theta^k)^2}[(\varepsilon_{i,j-1/2}^k\sin\theta_{j-1/2}^k)\tilde{P}_{i,j-1}^k - (\varepsilon_{i,j-1/2}^k\sin\theta_{j-1/2}^k + \varepsilon_{i,j+1/2}^k\sin\theta_{j+1/2}^k)\bar{P}_{i,j}^k + (\varepsilon_{i,j+1/2}^k\sin\theta_{j+1/2}^k)\bar{P}_{i,j+1}^k] - \frac{1}{(\Delta\phi^k)^2}[\varepsilon_{i-1/2,j}^k\tilde{P}_{i-1/2,j}^k - (\varepsilon_{i-1/2,j}^k + \varepsilon_{i+1/2,j}^k)\bar{P}_{i,j}^k + \varepsilon_{i+1/2,j}^k\bar{P}_{i+1,j}^k] + \sin^2\theta_j^k\left[\frac{1}{\omega}\frac{H_{i,j}^k - H_{i-1,j}^k}{\Delta\phi^k} + 2\frac{H_{i,j}^k}{\Delta T}\right] \tag{23}$$

$$\left(\frac{\partial L_{i,j}}{\partial P_{i,j}}\right)^k = -\frac{\sin\theta_j^k}{(\Delta\theta^k)^2}(\varepsilon_{i,j-1/2}^k\sin\theta_{j-1/2}^k + \varepsilon_{i,j+1/2}^k\sin\theta_{j+1/2}^k) - \frac{1}{(\Delta\phi^k)^2}(\varepsilon_{i-1/2,j}^k + \varepsilon_{i+1/2,j}^k) - \frac{(D_{0,0} - D_{1,0})\sin^2\theta_j^k}{\Delta\phi^k} - 2\frac{D_{0,0}\sin^2\theta_j^k}{\Delta T} \tag{24}$$

In Eqs. (21) and (23), $\bar{P}$ is the initial old pressure, and $\tilde{P}$ is the relaxed new pressure. At the beginning of every relaxation, H and ε were updated using the obtained $\tilde{P}$. W cycles were employed for pressure relaxation[26]. 257 nodes were arranged in both θ and ϕ directions on the finest level of grid according to previous studies[18,27]. Using formulae (25) and (26), ε_x and ε_y were first adjusted on the lowest level and then adjusted on the finest level after a W cycle when the relative error of pressure, defined in Eq. (27), was less than a given requirement, 0.05 in the present study.

$$\tilde{\varepsilon}_x = \bar{\varepsilon}_x - \omega_{\varepsilon_x}\left(\int_0^{\pi}\int_0^{\pi}\tilde{Q}\mathrm{d}\theta\mathrm{d}\phi - g_x\right) \tag{25}$$

$$\tilde{\varepsilon}_y = \bar{\varepsilon}_y - \omega_{\varepsilon_y}\left(\int_0^{\pi}\int_0^{\pi}\tilde{S}\mathrm{d}\theta\mathrm{d}\phi - g_y\right) \tag{26}$$

where ω_{ε_x} and ω_{ε_y} are the relaxation factors; $\bar{\varepsilon}_x$ and $\bar{\varepsilon}_y$ are the initial eccentricity ratios in the x and y directions respectively; and $\tilde{\varepsilon}_x$ and $\tilde{\varepsilon}_y$ are the modified eccentricity ratios.

The simulation started with a steady state solution. The convergent solution at an instant was obtained until the following requirements of pressure and loads were satisfied simultaneously on the finest level of grids:

$$\mathrm{Err}_P = \frac{\sum_{i=0}^{n_x}\sum_{j=0}^{n_x}|\tilde{P}_{i,j}^m - \bar{P}_{i,j}^m|}{\sum_{i=0}^{n_x}\sum_{j=0}^{n_x}\tilde{P}_{i,j}^m} < 0.001 \tag{27}$$

$$\mathrm{Err}_{\bar{f}_x} = \left|\frac{\bar{f}_x}{0.001W}\right| < 0.01 \tag{28}$$

$$\mathrm{Err}_{\bar{f}_y} = \left|\frac{W - \bar{f}_y}{W}\right| < 0.001 \tag{29}$$

where $\tilde{P}_{i,j}^m$ and $\bar{P}_{i,j}^m$ are the solved and initial pressures of a W cycle. The convergent solution of film thickness, pressure and eccentricities at this instant was used as the initial values for the next instant until five walking cycles were finished. Mesh sensitivity was checked for both spatial grid and temporal step to ensure the accuracy of the numerical prediction.

3 Results

Fig.4 shows the predicted central and minimum film thicknesses and maximum pressure as a function of time for an Alpharabola cup with $\alpha = 0.99$ during five walking cycles. It is clear that the cyclic convergence of the numerical solution was quickly achieved after two or three cycles. Therefore, all the results shown in Figs.5-8 were taken from the fifth walking cycle after the cyclic convergence was achieved. The typical three-dimensional film profiles and pressure distributions at the instants of 0.11 s, 0.5 s and 0.8 s of one convergent walking cycle are shown in Fig.5. Fig.6 shows the effect of α on quasi-static and transient solutions of the central and minimum film thicknesses and maximum pressures. Fig.7 compares the predicted central and minimum film thicknesses and maximum pressures between the transient solution and the quasi-static estimation of the Alpharabola cup with $\alpha = 0.9957$. In order to compare the lubrication performance of the Alpharabola cups with a spherical cup, the central and minimum film thicknesses and maximum pressure of a typical 28 mm spherical hip implant with a radial clearance of 30 μm are also plotted in Fig. 7 under both transient and quasi-static conditions. The comparison of the quasi-static and transient film profiles at the central line along the entraining direction at three instants with different values of α (0.9957, 0.97) is shown in Fig. 8.

4 Discussion

The film thickness in a transient EHL problem is

mainly determined by both the entraining and normal approach velocities. Moreover, the variation in both the load and the velocity may affect the normal approach velocity. Furthermore, the same walking condition may have different effects on lubrication performance for different bearing surfaces. The squeeze film action may also affect the pressure distribution although it is mainly determined by the loading conditions. Therefore, the lubrication mechanism in the Alpharabola prostheses is quite complex because of the complex walking conditions and aspherical bearing surfaces. In order to investigate the effect of the squeeze film action caused by the walking conditions, the transient solutions were compared with the quasi-static solutions. Moreover, the effect of the aspherical bearing surface was investigated by comparing both the quasi-static and transient solutions with those of a spherical one.

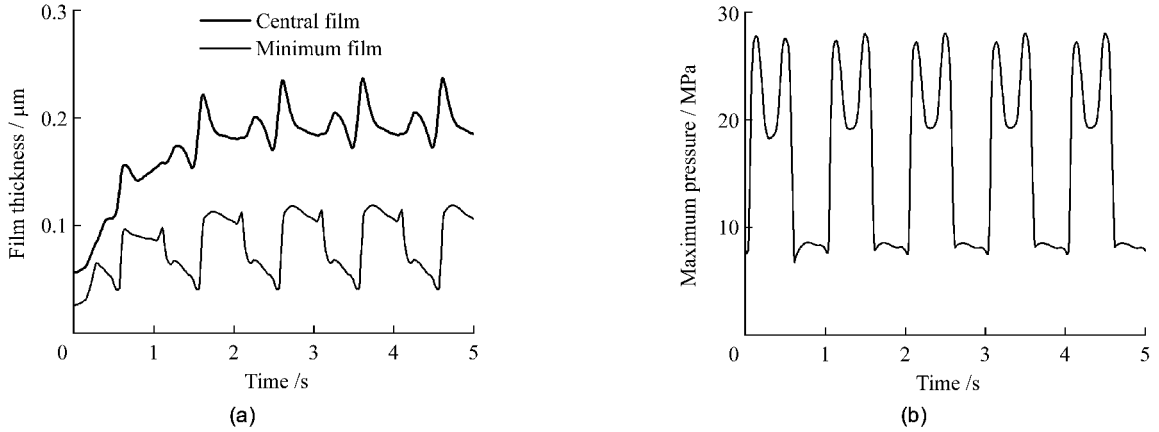

Fig.4 Predicted central and minimum film thicknesses (a) and maximum pressure (b) for an Alpharabola cup during five walking cycles (R_2 = 14 mm, α = 0.99)

图 4 一种 Alpharabola 型金属-金属人工髋关节在 5 个运动周期内的中心膜厚 (a)、最小膜厚 (b) 和最大压力(R_2 = 14 mm, α = 0.99)

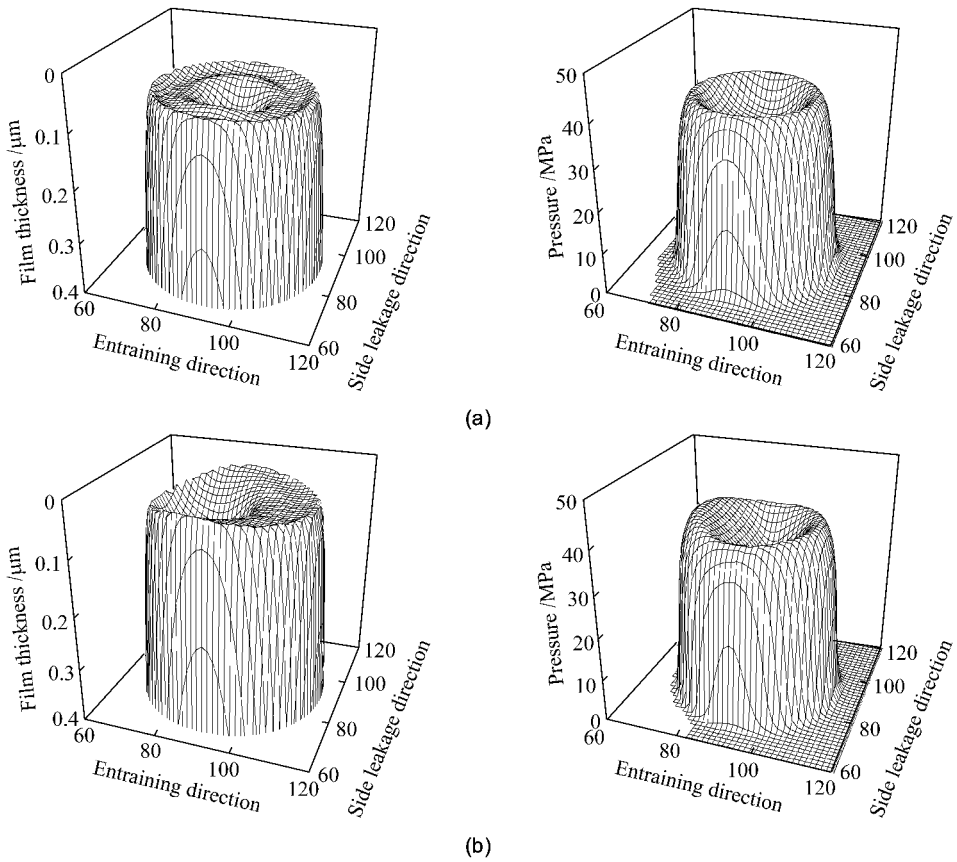

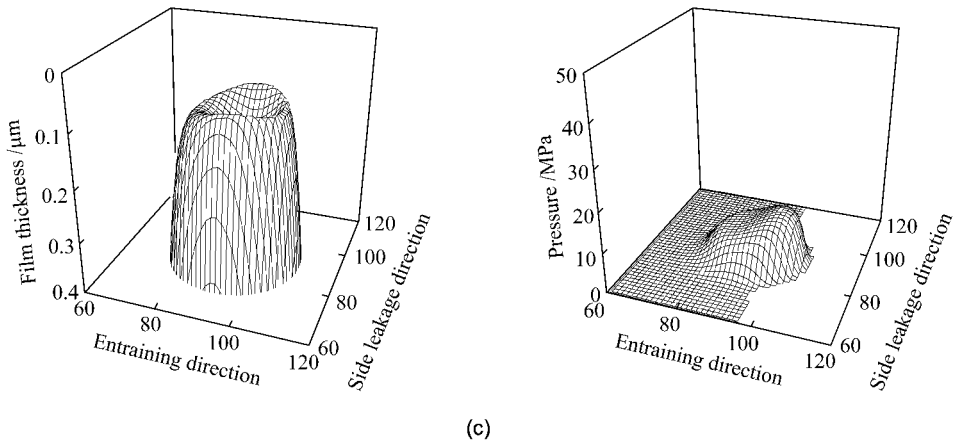

(c)

Fig.5 Film thickness profiles and pressure distributions at 0.11 s (a), 0.5 s (b) and 0.8 s (c) within a convergent cycle in an Alpharabola cup (R_2 = 14 mm, α = 0.97)

图 5 一种 Alpharabola 型金属-金属人工髋关节在一个收敛的周期内在第 0.11 秒 (a), 0.5 秒 (b) 和 0.8 秒 (c) 的油膜形状和压力分布 (R_2 = 14 mm, α = 0.97)

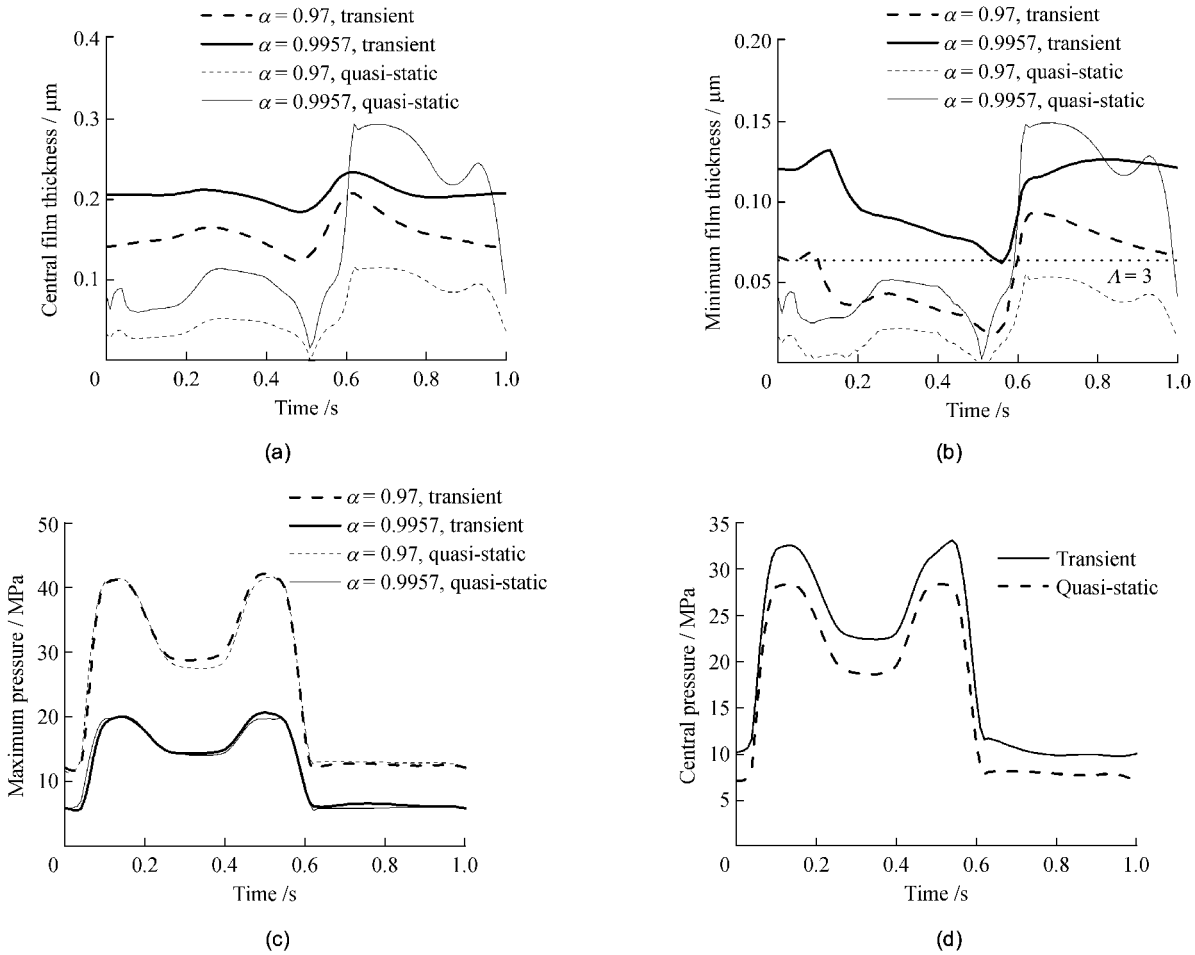

Fig.6 Predicted quasi-static solution and transient solution of central film thicknesses (a) minimum film thicknesses (b) and maximum pressures (c) for different Alpharabola cups (R_2 = 14 mm) and the comparison of central pressure between transient solution and quasi-static solution (d) of an Alpharabola cup (R_2 = 14 mm, α = 0.97) during one convergent cycle

图 6 在一个收敛的周期内,不同的 Alpharabola 髋臼的中心膜厚 (a)、最小膜厚 (b) 和最大压力 (c) 的准稳态解和时变解 (R_2 = 14 mm),及一种 Alpharabola 髋臼的中心压力的准稳态和时变解的对比 (d) (R_2 = 14 mm, α = 0.97)

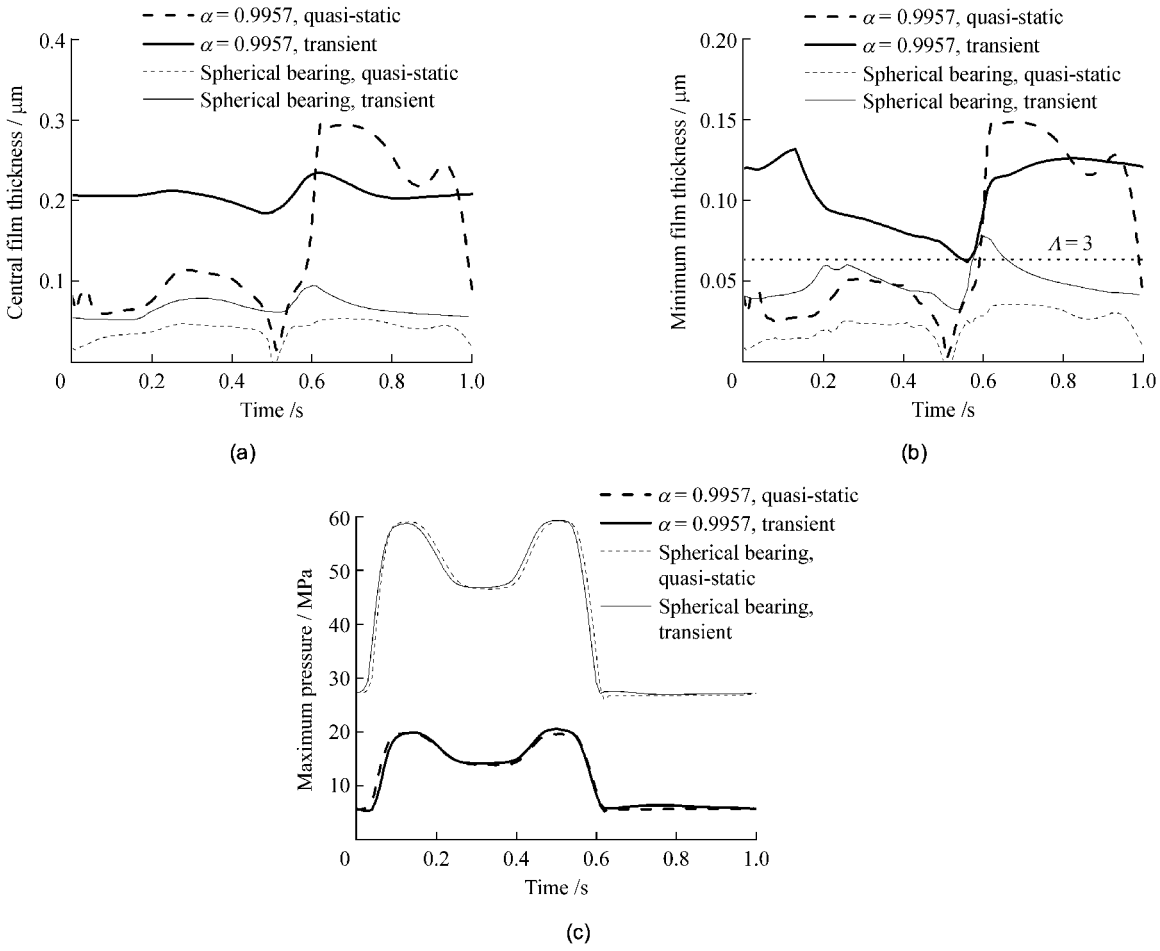

Fig.7 Predicted quasi-static solution and transient solution of central film thicknesses (a) minimum film thicknesses (b) and maximum pressures (c) for an Alpharabola cup (R_1 = 14 mm, α = 0.9957) and a spherical cup (R_1 = 14 mm, c = 30 μm) during one convergent cycle

图7 在一个收敛的周期内,Alpharabola 型人工髋关节 (R_1 = 14 mm, α = 0.9957) 和球型人工髋关节 (R_1 = 14 mm, c = 30 μm) 的中心膜厚 (a)、最小膜厚 (b) 和最大压力 (c) 的准稳态解和时变解的对比

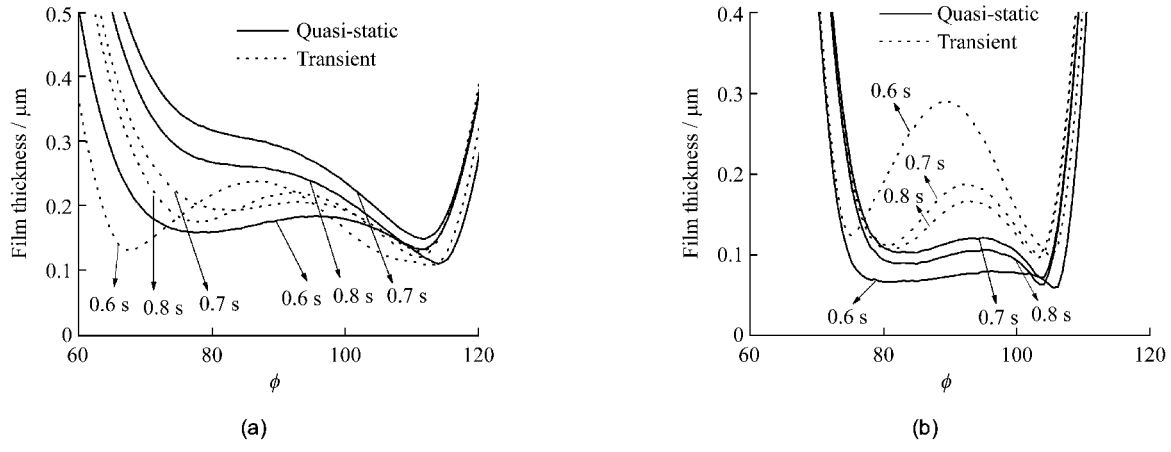

Fig.8 Quasi-static and transient film profiles at the central line along the entraining direction at three instants for Alpharabola cups of α = 0.9957 (a) and α = 0.97 (b) (R_2 = 14 mm)

图8 α = 0.9957 (a) 和 α = 0.97 (b) 的 Alpharabola 髋臼在卷吸速度方向上的中心线上的三个瞬时的油膜形状的准稳态解和时变解 (R_2 = 14 mm)

Compared with the spherical hip prostheses, the Alpharabola hip prosthesis featured a relatively uniform pressure distribution and a significantly thicker central film thickness during the whole walking cycle, as shown in Figs.5 and 8. The pocket in the film profile was similar to the dimple observed for a pure squeeze EHL problem[28]. Due to the nearly parallel bearing surfaces at the contact conjunction, the normal approach or separation velocities were much greater than those of the spherical bearing systems. Therefore, at the contact conjunction the squeeze film action of the Alpharabola hip prosthesis was much stronger, causing the dimple in film thickness profiles. The increased lubricant film at the contact center for the non-spherical cups may provide more protection from wear under adverse lubrication conditions such as a sudden increase in load or without entraining velocity, associated with start-up and stopping. Because of the strong squeeze film action at the contact area, the corresponding pressure was increased; therefore, a more uniform pressure distribution than the steady-state results[17] was formed. This may help to avoid the potential stress concentration caused by the annular maximum pressure distribution. Similar pressure distribution has also been found in the Metasul bearing system, as a result of the polyethylene backing[27].

As shown in Fig.6, during the stance phase, the squeeze film action of the transient walking conditions can significantly improve the film thickness. The transient central and minimum film thicknesses were generally two folds of the quasi-static results for both cases of α = 0.9957 and 0.97. However, during most of the swing phase, it is interesting to note that for the case of α = 0.9957, both the central and minimum film thicknesses under the quasi-static condition were thicker than those under the transient condition. However, for the case of α = 0.97, the transient film thicknesses were thicker. This is because for the case of α = 0.9957, the effect of entraining velocity under steady state condition was significant due to the more conforming bearing surfaces, as shown in Fig.8. However, under transient conditions, the damping of the lubricant prevented the film from varying directly with the entraining velocity. For the cup with α = 0.97, the effect of entraining velocity was overwhelmed by that of the squeeze film action during the swing phase. There was no large difference between the transient and quasi-static maximum pressures as shown in Fig.6c. However, the action of squeeze film on pressure occurred at the contact centre. A comparison between the transient and quasi-static central pressure indicates that the effect of transient action on pressure can not be neglected, as shown in Fig.6d. Therefore, steady-state EHL study is not enough to provide accurate estimation of film thickness and pressure distribution for the Alpharabola cup under real walking conditions. Correspondingly, the minimum film thickness formula developed by Hamrock and Dowson based on steady state, is no longer valid for this non-spherical cup due to the effects of squeeze film action and non-spherical surface.

Since the radii of the spherical head and the non-spherical cup were equal at the pole, the clearance between the head and cup was mainly produced by the variation in the radius of the cup. A smaller α means a greater deviation from a sphere, resulting in the decrease in the conformity in the contact area. Therefore, as shown in Fig. 6, with the decrease in α, the central and minimum film thicknesses decreased while the maximum pressure increased. This implies the importance of the sphericity of the bearing surfaces on lubrication performance and this is consistent with a previous study[29].

The effects of bearing surfaces and squeeze film action can be clarified individually by comparing the transient and quasi-static solutions of the Alpharabola cup and spherical cup systems. For example, as shown in Fig.7, at the instant of 0.1 s, the quasi-static solution of the Alpharabola hip prosthesis provided a minimum film thickness twice of that of the spherical bearing system because of the improved conformity. Furthermore, the transient solution of the spherical hip prosthesis was three folds of the corresponding quasi-static solution due to the large squeeze film action caused by the increase in load. However, the transient minimum film thickness of the Alpharabola hip prosthesis was more than six folds of that of the quasi-static solution of the spherical hip prosthesis. Therefore the synergistic effect of the squeeze film action and the conforming aspherical bearing surface is evident.

The lubrication performance of the Alpharabola cup and a spherical cup was compared by assuming a similar equatorial radial clearance. The corresponding α value for the non-spherical cup was 0.9957 to a 28 mm spherical cup with a radial clearance of 30 μm. Since the contact area of the Alpharabola hip prosthesis was greatly increased, compared with the spherical one under the same load [17], moreover, the pressure is mainly determined by load and contact area, the maximum pressure of the Alpharabola hip prosthesis during a walking gait was only 1/3 of that of the spherical hip prosthesis as shown in Fig.7. During most of a walking gait, both central and minimum film thicknesses of the Alpharabola hip prosthesis were more than two folds of those of the spherical one. Such a significant improvement in film thickness and decrease in pressure may be expected to reduce wear significantly.

It is interesting to estimate the mode of lubrication of the Alpharabola hip prosthesis. It has been shown that the 28 mm spherical MOM hip prosthesis with a radial clearance of 30 μm operates in a mixed lubrication regime, experimentally[30] and theoretically[20]. The theoretical prediction is usually based on the lambda ratio, which is defined as:

$$\Lambda = \frac{h_{\min}}{\sqrt{R_{a(\text{head})}^2 + R_{a(\text{cup})}^2}} \tag{30}$$

where $h_{\min}$ is the minimum film thickness during the walking cycle; $R_{a(\text{head})}$ and $R_{a(\text{cup})}$ are average roughness of femoral head and acetabular cup respectively, typically in the

rang of 5-15 nm[31]. A minimum value of three for Λ indicates a fluid film lubrication regime. The larger value of the roughness, 15 nm, resulting in a composite surface roughness of 21 nm, was adopted in this study to estimate the worse case scenario. As shown in Fig.7, the Alpharabola hip prosthesis with α of 0.9957 may operate in fluid film lubrication during the whole walking gait. However, for the 28 mm spherical hip prosthesis, fluid film lubrication only occurred 10% of a walking gait. Even for a α value of 0.97, corresponding to an equatorial clearance of 208 μm, fluid film lubrication may occur during the whole swing phase as shown in Fig.6, much higher than that in the spherical hip prosthesis. Therefore, the Alpharabola hip prosthesis is more likely to benefit from fluid film lubrication than the spherical hip prosthesis. This is consistent with the effect of the modified geometry after running-in wear on lubrication improvement[13, 14]. Therefore, it is expected that the Alpharabola hip prostheses may avoid or reduce the running-in wear phase.

There are a number of limitations of the present study. The anatomical inclination of the cup was not considered. When it is considered, the position of the zero clearance needs to be modified. A more realistic model should also include the abduction/adduction and internal/external motions and the load in *x* and *z* directions. Other important issues such as design and manufacturing of the non-spherical cup have not been addressed in this paper[17]. It should also be pointed out that predictions for Alpharabola hip prosthesis in this study need to be validated by further experimental studies, in terms of wear and friction test or the direct measurement of lubrication film.

5 Conclusion

A complete transient elastohydrodynamic lubrication numerical analysis was performed for a hip prosthesis with an aspherical acetabular cup under the dynamic load and motion specified by ISO standard. Detailed numerical method was presented. The effect of both squeeze film action and aspherical bearing on lubrication performance was investigated. It was found that both of these factors can increase lubricant film thickness. It was predicted that the Alpharabola hip prosthesis considered may be more likely to operate in a full fluid film regime, compared with spherical bearing surfaces. Moreover, it was also suggested that the running-in wear may be avoided or reduced by employing the Alpharabola acetabular cup.

Acknowledgment

This work was supported by the Overseas Research Students Award Scheme (ORSAS) to Qingen Meng, and the National Natural Science Foundation of China through grant 50628505. It is partly supported by the NIHR (National Institute for Health Research) as part of collaboration with the LMBRU (Leeds Musculoskeletal Biomedical Research Unit).

References:

[1] Sieber H, Reiker C, Kottig P. Analysis of 118 second generation metal-on-metal retrieved hip implants [J]. The Journal of Bone and Joint Surgery, British Volume. 1999, 81(1): 46-50.

[2] Doorn PF, Mirra JM, Campbell PA, *et al*. Tissue reaction to metal on metal total hip prostheses [J]. Clinical Orthopaedics and Related Research. 1996,329: S187-S205.

[3] Urban RM, Jacobs JJ, Tomlinson MJ, *et al*. Dissemination of wear particles to the liver, spleen, and abdominal lymph nodes of patients with hip or knee replacement [J]. The Journal of Bone and Joint Surgery, American Volume. 2000, 82(4): 457-477.

[4] Smith SL, Dowson D, Goldsmith AAJ. The lubrication of metal-on-metal total hip joints: a slide down the Stribeck curve [J]. Proceedings of the Institution of Mechanical Engineers, Part J: Journal of Engineering Tribology. 2001, 215(5): 483-493.

[5] Dowson D, Hardaker C, Flett M, *et al*. A hip joint simulator study of the performance of metal-on-metal joints, part II: design [J]. Journal of Arthroplasty. 2004,19 (8), S124-S130.

[6] Rieker CB, Schon R, Konrad R, *et al*. Influence of the clearance on in vitro tribology of large diameter metal-on-metal articulations pertaining to resurfacing hip implants [J]. Orthopedic Clinics of North America. 2005, 36 (2): 135-142.

[7] Liu F, Jin ZM, Hirt F, *et al*. Effect of bearing geometry and structure support on transient elastohydrodynamic lubrication of metal-on-metal hip implants [J]. Journal of Biomechanics. 2007,40(6), 1340-1349.

[8] Jagatia M, Jin ZM. Analysis of elastohydrodynamic lubrication in a novel metal-on-metal hip joint replacement [J]. Proceedings of the Institution of Mechanical Engineers, Part H: Journal of Engineering in Medicine. 2002,216(3): 185-193.

[9] Jin ZM, Meakins S, Morlock MM, *et al*. Deformation of press-fitted metallic resurfacing cups. part 1: experimental simulation [J]. Proceedings of the Institution of Mechanical Engineers, Part H: Journal of Engineering in Medicine. 2006,220(2): 299-309.

[10] Farrar R, Schmidt MB. The effect of diametral clearance on wear between head and cup for metal on metal articulations [C]. 43rd Annual Meeting of the Orthopaedic Research Society.

[11] Shen MC, Rieker CB, Gnepf P, *et al*. Effect of clearance on frictional torque characteristics of metal-on-metal THA [C]. 51st Annual Meeting of the Orthopaedic Research Society.

[12] Anissian HL, Stark A, Good V, *et al*. The wear pattern in metal-on-metal hip prostheses [J]. Journal of Biomedical Materials Research, Part B: Applied Biomaterials. 2001, 58(6): 673-678.

[13] Vassiliou K, Elfick AP, Scholes SC, *et al*. The effect of 'running-in' on the tribology and surface morphology of metal-on-metal Birmingham hip resurfacing device in simulator studies [J]. Proceedings of the Institution of Mechanical Engineers, Part H: Journal of Engineering in Medicine. 2006,220(2): 269-277.

[14] Liu F, Jin ZM, Hirt F, *et al*. Effect of wear of bearing surfaces on elastohydrodynamic lubrication of metal-on-metal hip implants [J]. Proceedings of the Institution of Mechanical Engineers, Part H: Journal of Engineering in Medicine. 2005,219(5): 319-328.

[15] Lee R, Essner A, Wang A. Tribological considerations in primary and revision metal-on-metal arthroplasty [J]. The Journal of Bone and Joint Surgery, American Volume. 2008,90(Suppl 3): 118-124.

[16] Fisher J. Acetabular Cup. World intellectual property organization patent[M], 1995, No. WO 95/23566.
[17] Meng QE, Gao LM, Liu F, *et al*. Contact mechanics and elastohydrodynamic lubrication in a novel metal-on-metal hip implant with an aspherical bearing Surface [J]. Journal of Biomechanics. 2009,In revision.
[18] Wang FC, Jin ZM. Transient elastohydrodynamic lubrication of hip joint implants [J]. ASME Journal of Tribology. 2008,130(1): 011007.
[19] Jagatia M, Jin ZM. Elastohydrodynamic lubrication of metal-on-metal hip prostheses under steady state entraining motion [J]. Proceedings of the Institution of Mechanical Engineers, Part H: Journal of Engineering in Medicine. 2001,215(6): 531-541.
[20] Jin ZM, Dowson D, Fisher J. Analysis of fluid film lubrication in artificial hip joint replacements with surfaces of high elastic modulus [J]. Proceedings of the Institution of Mechanical Engineers, Part H: Journal of Engineering in Medicine. 1997,211(3): 247-256.
[21] Yao JQ, Laurent MP, Johnson TS, *et al*. The influences of lubricant and material on Polymer/CoCr sliding friction [J]. Wear. 2003,255: 780-784.
[22] Bergmann G, Deuretzbacher G, Heller M, *et al*. Hip contact forces and gait patterns from routine activities [J]. Journal of Biomechanics. 2001,34(7): 859-871.
[23] ISO 14242-1. Implants for surgery-wear of total hip-joint prostheses-part 1: loading and displacement parameters for wear-testing machines and corresponding environmental conditions for test [M], 2002.
[24] Venner CH. Multigrid solution of the EHL line and point contact problems [D]. Ph.D. thesis, University of Twente, Enschede, the Netherlands, 1991.
[25] Wang FC, Jin ZM. Prediction of elastic deformation of acetabular cup and femoral head for lubrication analysis of artificial hip joints [J]. Proceedings of the Institution of Mechanical Engineers, Part J: Journal of Engineering Tribology. 2004, 218(3): 201-209.
[26] Jin ZM, Yang P, Cui J, *et al*. Transient elastohydrodynamic analysis of elliptical contacts. Part 1: isothermal and Newtonian lubricant solution [J]. Proceedings of the Institution of Mechanical Engineers, Part J: Journal of Engineering Tribology. 2004,218(3): 211-224.
[27] Liu F, Jin ZM, Hart F, *et al*. Transient elastohydrodynamic lubrication analysis of metal-on-metal hip implant under simulated walking conditions [J]. Journal of Biomechanics. 2006,39(5): 905-914.
[28] Dowson D, Wang D. An analysis of the normal bouncing of a solid elastic ball on an oily plate [J]. Wear. 1994,179 (1-2): 29-37.
[29] Wang FC, Jin ZM. Effect of non-spherical bearing geometry on transient elastohydrodynamic lubrication in metal-on-metal hip joint implants [J]. Proceedings of the Institution of Mechanical Engineers, Part J: Journal of Engineering Tribology. 2007,221(3): 379-389.
[30] Dowson D, McNie CM, Goldsmith AAJ. Direct experimental evidence of lubrication in a metal-on-metal total hip replacement tested in a joint simulator [J]. Proceedings of the Institution of Mechanical Engineers, Part J: Journal of Engineering Tribology. 2000,214(1): 75-86.
[31] Dowson D, Jin ZM. Metal-on-metal hip joint tribology [J]. Proceedings of the Institution of Mechanical Engineers, Part J: Journal of Engineering Tribology. 2006,220(2): 107-118.